RSC Advances

ROYAL SOCIETY OF CHEMISTRY

www.rsc.org/advances

Cite this: DOI: 10.1039/c0xx00000x

www.rsc.org/xxxxxx

ARTICLE TYPE

Interplay between the composition of LLDPE/PS blends and their compatibilization with polyethylene-*graft*-polystyrene in the foaming behaviour

Guangchun Zhang,[a,b] Yuanliang Wang,[a,b] Haiping Xing,[a] Jian Qiu,*[a] Jiang Gong,[a,b] Kun Yao,[a,b] Haiying Tan,[a,b] Zhiwei Jiang[a] and Tao Tang*[a]

Received (in XXX, XXX) Xth XXXXXXXXX 20XX, Accepted Xth XXXXXXXXX 20XX
DOI: 10.1039/b000000x

Polyethylene-*g*-polystyrene (PE-*g*-PS) copolymers, which were prepared by the combination of ROMP and ATRP method, were utilized to compatibilize LLDPE/PS blends. On one hand, the effect of PE-*g*-PS on morphologies of LLDPE/PS blends was investigated. On the other hand, the influences of branch length and added amount of PE-*g*-PS on the cell morphology of foamed LLDPE/PS blends with different composition were studied using supercritical CO_2 as physical foaming agent in a batch foaming process. It was found that the presence of PE-*g*-PS in the LLDPE/PS blends showed different influence on the foaming behaviour, strongly depending on the composition of the blends (i.e. the weight ratio of LLDPE and PS). How the interplay of compatibilization and composition of LLDPE/PS blends affected foaming behaviour of LLDPE/PS blends was studied. The reasonable explanation was ascribed to consecutive state of interfacial region, resulting from different phase structure of the blends. Compared to pristine LLDPE and PS, the blends with sea-island phase structure showed the improved foam morphology, but the presence of PE-*g*-PS did not strongly influence the foaming behaviours of these blends. In contrast, the presence of PE-*g*-PS dramatically promoted the foaming ability of LLDPE/PS blends with co-continuous phase structure. It was ascribed to the strengthened interfacial adhesion blocking the channel between two components through which CO_2 was released, and the viscoelasticity of the blends was not the key factor to determine the foaming behaviour under the same foaming conditions in this work.

Introduction

Fabricating polymer alloys through mixing different polymer components is a powerful method to prepare a new material different from its parental components. Owing to poor compatibility between most of different polymers, block or graft copolymers are often needed as compatibilizers in polymer blends. The compatibilization is important to stabilize morphology and promote the properties of the resultant blends.[1] Molecular structural parameters of block or graft copolymers play a key role in the compatibilization of polymer blends. Most of previous researches are mainly focused on the systems containing block copolymers as compatibilizer.[2-8] However, when using as compatibilizer, the presence of block copolymers increases melt viscosity of polymer blends due to its high molecular weight, so higher shear rate was required when melt processing takes place.[3, 9, 10] In contrast, graft copolymers with the same composition and total molecular weight displays a little increase in the melt viscosity at high shear frequency, although the melt viscosity of graft copolymers at lower shear frequency increases obviously.[11-13] Now there have been many reports about the compatibilization of immiscible polymer blends,[14-17] but few of them are focused on the effect of compatibilizers on foaming behaviour of polymer blends.

Fabricating foamed materials from polymer blends are fascinating and challenging in application and scientific research field, because foamed polymer blends afford the potential of combining the advantageous properties of each component within the foamed material, and take advantage of the multiphase characteristics for the foaming process. Apart from the basic foaming conditions (temperature, pressure et al.), composition of the blends as well as other additives could affect the material properties (such as crystallinity,[18] surface tension,[19, 20] melt strength,[21-23] solubility and diffusivity of CO_2[24]) and ultimately determine the foam morphology and properties.[25-31] For example, Rachtanapun et al.[32] have found that PP/HDPE = 30/70 blends, prepared by twin screw extruder at 100 rpm using CO_2 as blowing agent, exhibit poor foam morphology. The authors thought that higher HDPE content caused the matrix to be too soft (low viscous), leading to cell coalescence. Increasing the content of PP (50/50 and 70/30 blends), the blend foam shows improved morphology, due to viscosity and stiffness appropriate for the development of a microcellular structure.[33] The immiscible polymer blends show poor interface adhesion but pronounced surface activity, which favour cell nucleation. Rodrigue et al.[34] employed three-dimensional analysis to study

the interaction of foaming and blending in PP/HDPE blends during melt extrusion foaming using azodicarbonamide as blowing agent. Their results indicated that the foam morphologies of PP/HDPE blends were not substantially modified in the presence of compatibilizing agent (Kraton D 1102) except low dispersed phase concentration (10% and 90% PP). Zhai et al.[35] found that the addition of PP-*g*-PS copolymers could improve the foaming properties of PP/PS (50/50) blends due to the improved interfacial compatibility. They provided a direct experimental proof for the heterogeneous nucleation theory, i.e. most cells were located at the compatibilied interface due to low energy barrier for cell nucleation.

As we know, PE and PS are two kinds of common resins, which are widely applied in the foamed materials. However, the strength and stiffness of PE foam are low, and the toughness of PS foam is poor. It is a simple method to compensate the shortcoming by fabricating polymer blend of these two components. In order to prepare high-performance PE/PS blend foam, it is necessary to improve the interfacial interaction between PE and PS by adding compatibilizers. To our knowledge, the studies about foaming behaviour of compatibilized PE/PS blend were rare in the scientific literature, only a US patent[36] was related to this issue, in which the extrusion-foamed PE/PS blends using organic volatile blowing agent in the presence of hydrogenated styrene/butadiene block copolymers showed a good performance in the cushioning application. However, how the interplay of compatibilization and composition of PE/PS blends affects foaming behaviour of PE/PS blends is not studied.

In this work, PE-*g*-PS graft copolymers, which were prepared by the combination of ROMP and ATRP method (Scheme S1 in the supporting information), were utilized to compatibilize LLDPE/PS blends. Using supercritical CO_2 as physical foaming agent in a batch foaming, the influences of branch length and added amount of PE-*g*-PS on the cell morphology of foamed LLDPE/PS blends with different composition were studied. We found that the presence of PE-*g*-PS in the LLDPE/PS blends showed different influence on the foaming behaviour, strongly depending on the composition of the blends (i.e. the weight ratio of LLDPE and PS). It was focused on how the interplay of compatibilization and composition of LLDPE/PS blends affects foaming behaviour of LLDPE/PS blends.

Experimental section

2.1. Materials

Linear low density polyethylene (LLDPE, DFDA-7042, MI = 2.0 g/10min (ISO1133, 190 ^{o}C, 2.16 Kg), M_w = 141 Kg/mol, PDI = 3.3) was supplied by Sinopec Maoming Company, China. Polystyrene (PS, Polyrex® PG-383, MI = 3.0 g/10min (ISO1133, 200 ^{o}C, 5Kg), M_w = 372 Kg/mol, PDI = 1.7) was provided by Zhenjiang Chi Mei Chemical. Co., Ltd. Polyethylene-*g*-polystyrene (PE-*g*-PS) (used as a compatibilizer in this work) was synthesized through a method similar to the previous reports.[37, 38] The detail for the synthesis of PE-*g*-PS was provided in the supporting information.

2.2. Preparation of LLDPE/PS blends

All blend samples were prepared by solution mixing method. The LLDPE with butylated hydroxytoluene (BHT) was first dissolved in refluxing toluene and kept under N_2 atmosphere to prevent oxidation. The PE-*g*-PS and PS were subsequently added to the above hot solution. After the mixture formed a clear and homogeneous solution, the blend was precipitated into methanol, and dried under vacuum before melt pressed.

2.3. Batch foaming

A stainless steel high-pressure vessel was used in batch foaming process. The high-pressure vessel was loaded with sample granules. After the high-pressure vessel was purged with low-pressure CO_2, a given amount of CO_2 was pumped into the vessel. The vessel was heated to predetermined foaming temperature and continuously charged with CO_2 to the fixed pressure. The samples were saturated for 4 h to ensure equilibrium adsorption of CO_2. Thereafter, the valve was rapidly opened to release the CO_2. Then the high-pressure vessel was opened up, and the foamed samples were taken out for subsequent analyses.

2.4. Characterization methods

The morphology of polymer blends was characterized by a XL 30 ESEM FEG scanning electron microscope (SEM). The compression-molded blend samples were cryofractured in liquid nitrogen. The fractured surfaces were coated with a thin layer of gold before SEM observation.

The cell morphology of the foamed samples was characterized by an XL 30 ESEM FEG scanning electron microscope (SEM). The foamed samples were fractured in liquid nitrogen and SEM images of the fractured surfaces were taken. A representative micrograph containing 100 to 200 bubbles was obtained and the number of bubbles n in the micrograph was determined. The cell diameter was the average of the sizes of more than 100 cells on the SEM micrograph. The cell density (N_0), the number of cells per cubic centimeter of solid polymer, was determined from Eq. (1):

$$N_0 = \left[\frac{n}{A}\right]^{3/2} \frac{\rho}{\rho_f}$$

where n is the number of cells seen in the SEM micrograph; A is the area of the micrograph (cm^2), calculated according to the scale bar, ρ and ρ_f are the mass densities of samples before and after foaming treatment, respectively, which was measured by water displacement method.

Rheological measurements were performed on a rotation rheometer ARES G2 at 180 ^{o}C. The parallel plate with a diameter of 25 mm and a gap height of 0.8 mm was used. The test samples were first treated with 0.2 wt % Irganox B215 antioxidant and formed into disks with a diameter of 25 mm and a thickness of 1 mm by compression-molding at 180 ^{o}C and 10 MPa. Then, the samples were quenched at room temperature. The range of the frequency sweeps was from 0.05 to 200 rad/s, and a strain of 1% was used, which was in the linear viscoelastic region for all samples. The rheometer oven was purged with dry nitrogen to avoid degradation of samples during measurements.

Results and discussion

3.1. The effect of PE-*g*-PS on the morphologies of LLDPE/PS blends

PE-*g*-PS graft copolymers with different branch length (Table 1) were utilized to compatibilize LLDPE/PS blends prepared by solution mixing. Figure 1 illustrates SEM micrographs of cryogenic fractured surfaces of LLDPE/PS=70/30 (by weight) blends with various amount of PE-*g*-PS. The dispersed PS particles and holes were evidently observed in the binary LLDPE/PS blend (Figure 1a). This indicates poor interfacial adhesion between PS and LLDPE matrix. However, the morphology was remarkably different from the binary blend when an amount of PE-*g*-PS copolymers was added regardless of branch length (Figure 1b-1j). The LLDPE/PS/PE-*g*-PS blends showed flat fractured morphology, indicating enhanced interfacial adhesion between PS and LLDPE. Figure 1e-1g show the morphologies of the LLDPE/PS/PE-*g*-$PS_{1.09k}$ blend with the loading of PE-*g*-PS at 1.0, 2.5, 5.0 wt%, respectively. The average size of PS dispersed particles reduced with the concentration of the compatibilizer (Figure S3a in the supporting information), which is in accordance with the prediction of the previous report.[14] Furthermore, it can also be seen that the compatibilization of PE-*g*-PS promotes with the length of PS chains (Figure S3b).

Table 1. Summary of the molecular characteristics of PE-Br and PE-*g*-PS copolymers with different branch length.

Run	M_{wSEC} (Kg mol^{-1})	PDI	St content		Branch density[a]	Branch Length (Kg mol^{-1})
			mol%	wt%		
			^{1}H-NMR			
PE-Br	73.5	1.82	—	—	54	—
1	74.8	1.84	3.12	10.69	54	0.34
2	80.5	1.94	9.59	28.24	54	1.09
3	82.2	1.95	13.44	36.57	54	1.59

[a] the average number of branch chain per 10000 backbone carbon atoms.

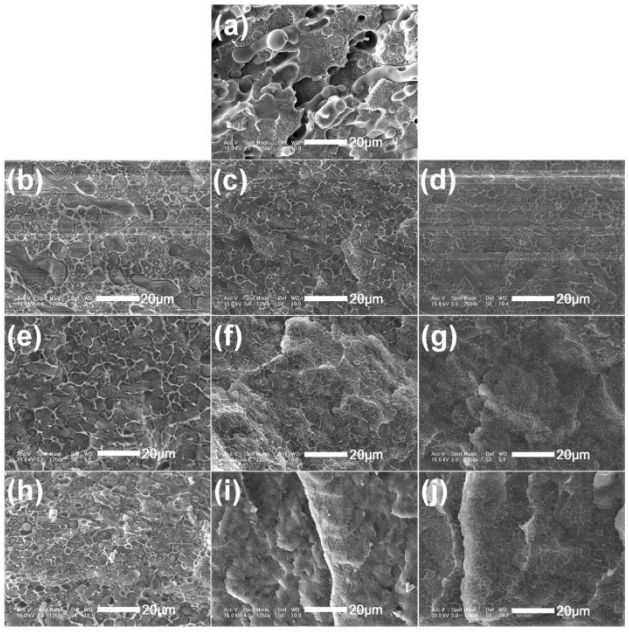

Figure 1. SEM images for binary LLDPE/PS (70/30) (a) and the compatibilized blends containing PE-*g*-PS with different branch length at different loadings of 1.0, 2.5, 5.0 wt% ((b)-(d) for PE-*g*-$PS_{0.34k}$, (e)-(g) for PE-*g*-$PS_{1.09k}$ and (h)-(j) for PE-*g*-$PS_{1.59k}$).

3.2. The effect of graft copolymers on foaming behaviours of LLDPE/PS = 70/30 blends

Figure 2a and 2b show the cell morphologies of LLDPE and PS foams obtained using supercritical CO_2 as foaming agent under a batch foaming process (13.3 MPa CO_2 pressure at 113 ^oC). Both foams of LLDPE and PS exhibited large cell size (D_c) and small cell density (N_o) (Table 2). Figure 2c shows the morphology of foamed LLDPE/PS=70/30 blend. Very surprisingly, this binary LLDPE/PS blend was almost unfoamed (expansion ratio=1.1). Furthermore, compared to the fractured surface morphology of unfoamed LLDPE/PS=70/30 blend (Figure 1a), the interfacial gap between two components in the foaming-processed blends became larger. Interestingly, the blends compatibilized by 1.0 wt% PE-*g*-$PS_{0.34k}$ exhibited fully foamed morphology (Figure 2d), and the expansion ratio increased to 4.8. Compared to both LLDPE and PS, the cell diameter (D_c) of LLDPE/PS/PE-*g*-$PS_{0.34k}$ 70/30/1.0 decreased to ~10 μm, and the cell density (N_o) increased to 4.7×10^9 cells/cm^3 (Table 2). It is clear that the introduction of PE-*g*-$PS_{0.34k}$ can effectively improve the foaming behaviour of LLDPE/PS=70/30 blend. The influence of PE-*g*-$PS_{0.34k}$ loading on the foaming behaviour of LLDPE/PS=70/30 blend was also investigated. The increase of PE-*g*-$PS_{0.34k}$ content could further improve the foaming behaviour of LLDPE/PS/PE-*g*-$PS_{0.34k}$ (Figure 2e-2f). When the content of PE-*g*-$PS_{0.34k}$ increased from 1.0 to 5.0 wt%, the expansion ratio increased from 4.8 to 6.7, the cell D_c was about 9~10 μm, and the cell density N_o was increased to 8.8×10^9 cells/cm^3. We also observed that, although PE-*g*-$PS_{0.34k}$ was added only 1.0 wt%, the overall foam structure was basically uniform (Figure 2d). When the content of PE-*g*-$PS_{0.34k}$ increased to 5.0 wt%, the foam morphology became more uniform so we could not distinguish the foam districts from LLDPE and PS (Figure 2f).

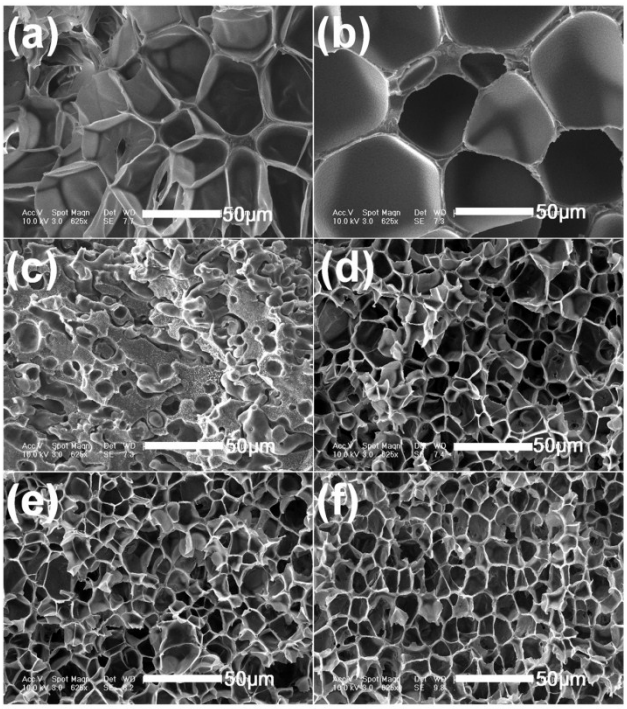

Figure 2. SEM images for cell morphologies of (a) LLDPE, (b) PS, (c) LLDPE/PS (70/30) blend and that with PE-*g*-$PS_{0.34k}$ added as

compatibilizers (d) (70/30/1.0), (e) (70/30/2.5) and (f) (70/30/5.0) foams. Foaming temperature: 113 °C; CO_2 saturation pressure: 13.3 MPa.

Table 2. Summary of the cell parameters of foamed LLDPE/PS=70/30 blends with or without compatibilizers.

Sample		D_d[a] (μm)	Expansion ratio	D_c[b] (μm)	N_o[c] (10^9 cells cm^{-3})
LLDPE		—	2.7	18.7	0.286
PS		—	5.6	50.9	0.058
LLDPE/PS 70/30		14.7	1.1	—	—
LLDPE/PS/ PE-*g*-$PS_{0.34k}$	70/30/1.0	4.84	4.8	10.5	4.69
	70/30/2.5	4.70	5.5	9.6	6.91
	70/30/5.0	4.06	6.7	10.1	8.81

[a] Mean droplet diameter. [b] Average cell diameter. [c] Cell density.

Figure 3 exhibits the SEM micrographs of foamed LLDPE/PS (70/30) blends (under the conditions: T = 110 °C and P = 13.3 MPa) compatibilized by PE-*g*-$PS_{0.34k}$, PE-*g*-$PS_{1.09k}$ and PE-*g*-$PS_{1.59k}$, respectively. Here the foaming temperature (T = 110 °C) was lower than the previous one (T = 113 °C), but the pressure kept the same. From Figure 3a-3c, it could also be seen that increasing the content of PE-*g*-$PS_{0.34k}$ resulted in an improved foaming behaviour (the cell parameters were summarized in Table 3) even though the foaming conditions were changed. Comparing the foaming results at different foaming temperatures (Table 2 vs Table 3), it was found that the cell density increased and the cell size decreased at a lower foaming temperature. Decreasing the temperature will increase the viscosity of the substrate material, causing the force restricting cell growth to increase and the diffusivity of CO_2 within the substrate to decrease.[39,40] If the CO_2 diffusivity decreases, the sorption of CO_2 during CO_2 dissolution decreases, thus, the quantity of CO_2 in the sample is lower than samples treated at higher temperatures.[41] These factors lead to decreased cell size. Decreased temperature results in a higher degree of swelling by CO_2 and thus the formation of more nuclei, which increases cell density[39,40]. The cell density of compatibilized blends was improved with the increase of the content of PE-*g*-$PS_{0.34k}$ or PE-*g*-$PS_{1.09k}$. However, when the content of PE-*g*-$PS_{1.59k}$ increased from 1.0 wt% to 5.0 wt%, the cell density slightly changed. There are following possible reasons for weak dependence of the cell density on the content of PE-*g*-$PS_{1.59k}$. On one hand, the cell density of the blend sample containing 1.0 wt% PE-*g*-$PS_{1.59k}$ is much higher than those of the counterparts containing PE-*g*-$PS_{0.34k}$ or PE-*g*-$PS_{1.09k}$, which results from the better compatibilization of PE-*g*-$PS_{1.59k}$ due to the presence of long PS branches. On the other hand, the addition of more PE-*g*-$PS_{1.59k}$ can reduce the average droplet diameter (Table 3), so the heterogeneous nucleation sites provided by the interfaces between the dispersed PS droplets and the LLDPE matrix should increase. Theoretically speaking, the cell density of the blends will increase. Thus, the possible reason is the reduction of the nucleation efficiency during foaming process in the case containing 5 wt% PE-*g*-$PS_{1.59k}$, which results in the reduction of cell density.[42] In summary, the compatibilized LLDPE/PS (70/30) blends exhibited improved foaming ability (such as higher expansion ratio, increased cell density and reduced cell size) compared to pure LLDPE, PS and the corresponding binary blend.

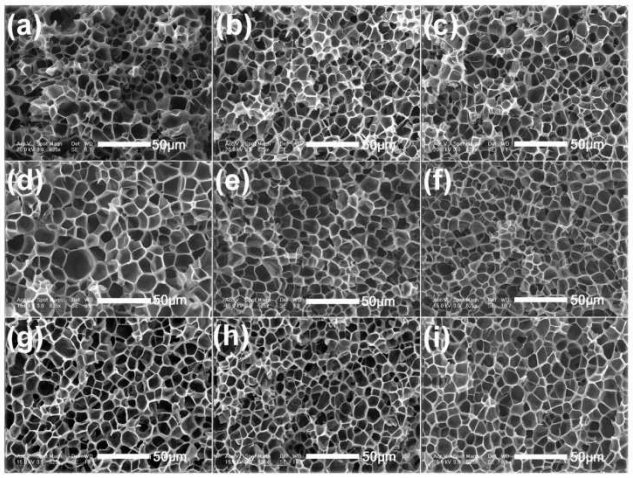

Figure 3. SEM micrographs for foamed morphologies of LLDPE/PS blends with PE-*g*-$PS_{0.34k}$ at different mass ratios 70/30/1.0 (a), 70/30/2.5 (b) and 70/30/5.0 (c), with PE-*g*-$PS_{1.09k}$ at different mass ratios 70/30/1.0 (d), 70/30/2.5 (e) and 70/30/5.0 (f), with PE-*g*-$PS_{1.59k}$ at different mass ratios 70/301.0 (g), 70/30/2.5 (h) and 70/30/5.0 (i) foams. Foaming temperature: 110 °C; CO_2 saturation pressure: 13.3 MPa.

Table 3. The cell parameters of LLDPE/PS blends (70/30) with or without compatibilizers after foaming (Figure 3). Foaming conditions: foaming temperature: 110 °C; CO_2 saturation pressure: 13.3 MPa.

Sample		D_d[a] (μm)	Expansion ratio	D_c[b] (μm)	N_o[c] (10^9 cells cm^{-3})
PE/PS 70/30		14.7	1.1	—	—
LLDPE/PS/ PE-*g*-$PS_{0.34k}$	70/30/1.0	4.84	2.7	6.9	4.56
	70/30/2.5	4.70	4.7	7.5	9.20
	70/30/5.0	4.06	5.3	7.8	11.2
LLDPE/PS/ PE-*g*-$PS_{1.09k}$	70/30/1.0	4.57	5.8	10.7	5.60
	70/30/2.5	3.47	5.2	9.3	7.78
	70/30/5.0	1.75	5.5	8.1	11.0
LLDPE/PS/ PE-*g*-$PS_{1.59k}$	70/30/1.0	3.66	5.2	8.8	8.44
	70/30/2.5	2.40	4.4	7.8	9.76
	70/30/5.0	1.74	5.6	9.1	9.00

[a] Mean droplet diameter; [b] Average cell diameter; [c] Cell density.

3.3 The effect of blend composition on foaming behaviours of uncompatibilized and compatibilized LLDPE/PS blends

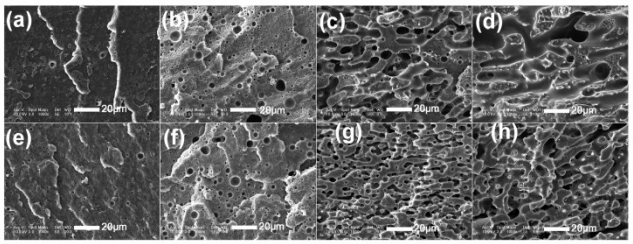

Figure 4. SEM images for etched by THF LLDPE/PS (90/10) (a), 80/20 (b), 60/40 (c), 50/50 (d), and with PE-*g*-$PS_{0.34k}$ as compatibilizers at the same loadings 90/10/1.0 (e), 80/20/1.0 (f), 60/40/1.0 (g), and 50/50/1.0 (h).

The influence of PE-*g*-PS on the foaming behaviours of blends with different compositions was further investigated, mainly via changing the weight ratio of LLDPE/PS from 90/10 to 50/50 while keeping the content of PE-*g*-$PS_{0.34k}$ (1.0 wt%). Figure 4 shows the influence of PE-*g*-PS on the morphology of LLDPE/PS blends with various compositions before foaming processing. The

samples were etched by THF to remove PS component before SEM observation. It can be seen that the size of dispersed PS particles does not reduce remarkably in the cases of LLDPE/PS=90/10 and 80/20 in the presence of PE-*g*-PS. When the content of PS increased to 40 and 50 wt%, the blends exhibited co-continuous phase structure. In these cases, the addition of PE-*g*-PS dramatically improved the dispersion states of both components.

Figure 5 shows foam morphologies of the above blends. As shown in Figure 5a, the LLDPE/PS=90/10 binary blend showed fully foamed morphology. Compared to pure LLDPE, the expansion ratio increased to 8.1, the cell size decreased to 14.4 μm, and the cell density increased to 3.03×10^9 cells/cm^3 (Table 4). However, the addition of PE-*g*-PS$_{0.34k}$ in this binary blend did not remarkably improve the foaming behaviour (Figure 5e, and cell parameters in Table 4) comparing with the foam morphology of the pure binary blend. A similar changing trend was observed in LLDPE/PS=80/20 blend after adding 1.0 wt% PE-*g*-PS$_{0.34k}$ (Figure 5b and 5f, and Table 4). Obviously, blending can lead to a significant increase in cell density compared to pure LLDPE, indicating that the cell nucleation is strongly influenced by the dispersion state of PS phase and the morphology of the blend. The addition of a small amount of PS (10 to 20 wt%) significantly increases the cell density, resulting from a heterogeneous nucleation effect of dispersed PS phase, which

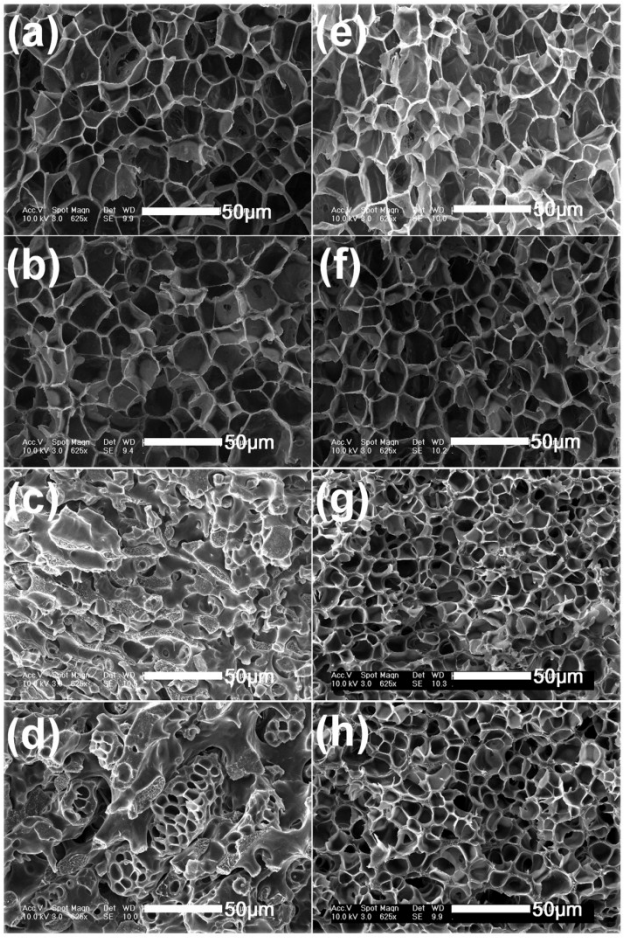

Figure 5. SEM images for cell morphologies of LLDPE/PS blends with the composition of 90/10 (a), 80/20 (b), 60/40 (c) and 50/50 (d), with PE-*g*-PS$_{0.34k}$ as compatibilizers at the same content 1.0wt% 90/10/1.0 (e), 80/20/1.0 (f), 60/40/1.0 (g), and 50/50/1.0 (h). The samples were treated under the same foaming batch conditions.

dominates over the homogeneous nucleation under the foaming conditions. The addition of graft copolymers did not change the average size of PS droplets so much (Figure 4e and 4f), indicating that the heterogeneous nucleation sites provided by the interfaces between the dispersed PS droplets and the LLDPE matrix kept almost constant. As a result, the cell density did not change so much in the presence of graft copolymer.

Similar to the case of LLDPE/PS 70/30 binary blend, the LLDPE/PS 60/40 binary blend did not form the foam structure as well (Figure 5c). The addition of 1 wt% PE-*g*-PS$_{0.34k}$ dramatically improved the foaming behaviour of LLDPE/PS 60/40 blend (Figure 5g), which is similar to the aforementioned cases of LLDPE/PS/PE-*g*-PS$_{0.34k}$ 70/30/1.0 vs LLDPE/PS 70/30 (Figure 2c and 2d). From Table 4, the average cell size was 7.1 μm in LLDPE/PS/PE-*g*-PS$_{0.34k}$ 60/40/1.0, the cell density was 5.27×10^9 cells/cm^3. It was of interest that the binary LLDPE/PS=50/50 blend displayed distinct fractured morphology (Figure 5d), in which the foamed regions belonged to the PS phase, and the unfoamed regions came from the LLDPE phase (from the etched foam morphology in Figure 6). Similarly, when 1.0 wt% PE-*g*-PS$_{0.34k}$ was added, the compatibilized blends exhibited fully foamed morphology. In a word, the presence of PE-*g*-PS could dramatically improve foaming capacity of LLDPE/PS blends with co-continuous phase structure. The foaming results of LLDPE/PS blends with the composition from 40/60 to 10/90 with PE-*g*-PS$_{1.59k}$ also supported the above conclusion (Figure S4 and S5 in the supporting information). The observed phenomenon in this work is different from the previous reports.[34] This difference might result from the different polymer blends or different foaming processes, which need to be more studied.

Table 4. Summary for the cell parameters of foamed LLDPE/PS blends with or without compatibilizers.

Sample	Expansion ratio	D_c (μm)	N_o(10^9 cells cm^{-3})
LLDPE	2.7	18.7	0.286
PE/PS 90/10	8.1	14.4	3.03
PE/PS/PE-*g*-PS$_{0.34k}$ 90/10/1.0	8.7	13.9	3.66
PE/PS 80/20	6.2	13.4	3.03
PE/PS/PE-*g*-PS$_{0.34k}$ 80/20/1.0	6.5	13.4	3.22
PE/PS 70/30	1.1	—	—
PE/PS/PE-*g*-PS$_{0.34k}$ 70/30/1.0	4.8	10.5	4.69
PE/PS 60/40	1.4	—	—
PE/PS/PE-*g*-PS$_{0.34k}$ 60/40/1.0	3.4	7.1	5.27
PE/PS 50/50	1.4	—	—
PE/PS/PE-*g*-PS$_{0.34k}$ 50/50/1.0	3.6	7.3	5.79
PE/PS 40/60	1.2	—	—
PE/PS/PE-*g*-PS$_{1.59k}$ 40/60/1.0	5.4	10.1	6.58
PE/PS 30/70	1.4	—	—
PE/PS/PE-*g*-PS$_{1.59k}$ 30/70/1.0	5.4	8.0	9.79
PE/PS 20/80	5.5	9.9	5.36
PE/PS/PE-*g*-PS$_{1.59k}$ 20/80/1.0	6.2	8.8	8.72
PE/PS 10/90	5.8	9.4	5.37
PE/PS/PE-*g*-PS$_{1.59k}$ 10/90/1.0	4.7	8.5	7.05
PS	5.6	50.9	0.058

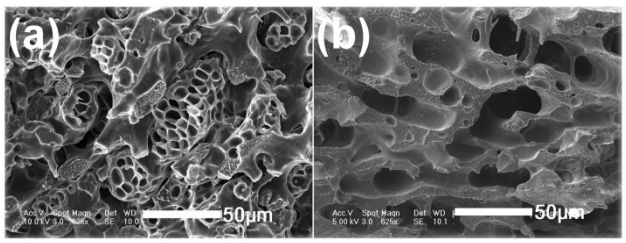

Figure 6. SEM micrographs for cryogenic fractured LLDPE/PS (50/50) after foaming process (a) and further etched surface by THF (b).

In order to further study the foaming behaviour of LLDPE/PS blends with various compositions before and after compatibilized by PE-*g*-PS, we decreased the foaming temperature to 100 °C, and kept CO_2 pressure (13.3 MPa) and saturation time constant. The influence of foaming temperature on the foam morphology is quite complex since it influences the gas solubility, nucleation rate as well as polymer viscosity. From Figure 7, it can be seen that LLDPE did not foam and PS can foam expectedly under this foaming condition. When a small amount of PS was added into the LLDPE (10-20 wt%), the foaming capacity of LLDPE/PS blends was significantly improved (Figure 7c and 7e). This indicates that the dispersed PS particles in LLDPE matrix act as nucleation agents for the foaming process of LLDPE. In this case, the addition of PE-*g*-PS can further increase the cell density. However, when the content of PS was 30-50 wt%, the binary LLDPE/PS blends presented very poor foaming behaviour. There were a lot of gaps in the interfacial region between two components (Figure 7g, 7i and 7k). These gaps were larger than those of unfoamed samples. This means that a lot of CO_2 was released through the interfacial region.

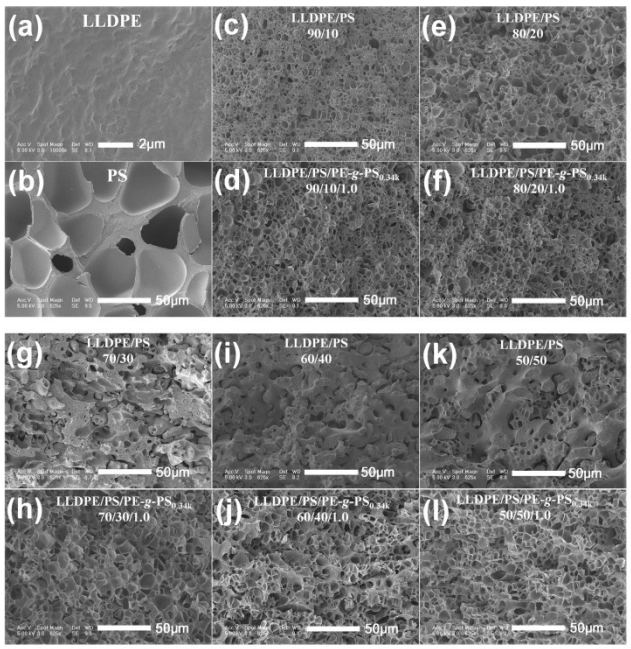

Figure 7. SEM images for the foamed LLDPE/PS blends with various composition before and after compatibilized by PE-*g*-PS (the foaming temperature: 100 °C, and kept CO_2 pressure and saturation time the same as the foaming conditions shown in Figures 2 and 5).

3.4 Insight into the influence of PE-*g*-PS on foaming behaviours of LLDPE/PS blends with different composition

According to the above results, it can be seen that the compatibilization of PE-*g*-PS play a different role in the foam morphologies of LLDPE/PS with various compositions. What is the mechanism behind the foaming behaviour of compatibilized LLDPE/PS blends with different composition? It is well known that the cell morphology is influenced by the nucleation of bubbles and their growth during the foaming process. Compared to single polymer, there are more factors influencing the foaming process of polymer blends, not only including gas solubility in the material, the rate of gas loss (diffusivity) and rheological properties of polymer materials, but also multiphase structure and interfacial region between different components. The CO_2 gas uptake in the blend materials depends on the composition (and crystallinity in the blends containing crystalline component) of blends under the fixed foaming processing conditions. The presence of a small amount of PE-*g*-PS does not obviously change the weight ratio of LLDPE to PS. The influence of added PE-*g*-PS on crystalline properties (such as crystallinity and crystal form) of PE component in the blends was investigated by means of DSC and WAXD measurements (Figure S6 and S7). The results showed that the addition of PE-*g*-PS did not show an obvious effect on the crystallinity and crystal form of LLDPE component in the blends. Interestingly, compared to the unfoamed samples, all the foamed samples presented double melting peaks and a slightly high crystallinity of LLDPE component in the blends (the crystallinities for unfoamed LLDPE/PS=60/40 and foamed LLDPE/PS=60/40 were 36.8% and 39.5%, respectively) despite the presence of PE-*g*-PS. Moreover the crystallinity of LLDPE component in the foamed binary blends and compatibilized blends were very close (the crystallinities of 39.5% and 38.3% for foamed LLDPE/PS=60/40 and foamed LLDPE/PS/PE-*g*-$PS_{0.34k}$=60/40/1.0, respectively, calculated by DSC). Thus the crystalline properties of the blends are not a key factor to the obvious difference of foaming behaviour between the binary blends and the compatibilized blends. Other factors, such as rheological properties, phase morphology and interfacial adhesion, might determine the difference in foaming behaviour and cell morphologies of LLDPE/PS binary blend and compatibilized LLDPE/PS blend, especially the last two factors among which affects the diffusion process of CO_2. In this work, the rheological measurements showed that the complex viscosity (η^*) and storage modulus (G') of LLDPE/PS (70/30) was higher than pure LLDPE and lower than PS (Figure S8 in the supporting information). This indicated that the viscoelasticity of the binary blends was in between LLDPE and PS. Because both LLDPE and PS can be foamed under the fixed foaming conditions, naturally it is expected that the binary blends should be foamed under the same foaming conditions. However, the foaming result indicated that the foaming behaviour of the binary LLDPE/PS (70/30) blend was very poor. Furthermore, although the complex viscosity (η^*) and storage modulus (G') of LLDPE/PS/PE-*g*-$PS_{0.34k}$=70/30/1.0 was almost the same as LLDPE/PS=70/30 (Figure S8), the foam morphologies of both the samples were totally different. These results demonstrated that the viscoelasticity of the samples is not the key factor to determine the foaming behaviour among these samples under the same foaming conditions.

It is well known that various phase structures can be developed

when two immiscible polymers are mixed together to make polymer blends, depending on the composition and viscosity ratio of two components. Particularly, in the case of LLDPE/PS blends, the phase morphology will change from sea-island to co-continuous phase structure and to sea-island phase structure again with increasing the content of PS. Whether the interfacial region is consecutive or not is related to the phase structure of LLDPE/PS blends. The interfacial region is isolated in the blends with sea-island phase structure. Otherwise, the interfacial region is consecutive in the blends with co-continuous phase structure (Figure S9). Generally, the presence of void fraction has a strong effect on the diffusivity more than the solubility of gas in the polymer materials.[27] Zhai et al. have found that the diffusion coefficients of CO_2 for all PP/PS (50/50) blends are higher than those of the two pure polymers.[35] It is believed that the diffusion coefficients of CO_2 in LLDPE/PS=70/30 blend with irregular dispersed morphology (not spherical dispersed morphology) or LLDPE/PS=50/50 blend (co-continuous phase structure) will also increase relative to the LLDPE or PS. According to the classical nucleation theory, CO_2 tend to assemble at the interface due to lower energy barrier, once depressurizing the consecutive interfacial region provided channels through which the assembled CO_2 diffuse from the bulk to the environment rapidly and no CO_2 left for cell growth. The enlarged gaps between two components in the foamed LLDPE/PS=70/30 (or 50/50) blend provided the evidence of CO_2 escaping from the interfacial region. As a result, LLDPE/PS blends with the composition of 70/30-30/70 could not efficiently form cell structures during the foaming process.

In contrast, when the composition of LLDPE/PS blends was 90/10, 80/20, 20/80 or 10/90, the blends showed a typical of sea-island phase structure (Figure 4a and 4b, and Figure S4c and S4d), that is, spherical dispersed phase was distributed in the matrix, therefore, the interfacial regions are isolated from each other in the blends. In this case, the enriched foaming gas in the interfacial region could not be released rapidly to the environment due to the presence of the continuous phase outside the interfacial region. So the foam structure could be formed under the same foaming conditions. Figure S10 in the supporting information showed that there were unfoamed particles (LLDPE particles) left in the foamed LLDPE/PS 20/80 blends after etching the sample by THF at room temperature. This indicated that the foamed structure was composed of PS component (continuous phase), and LLDPE as dispersed phase was not foamed. It is well known that the poorly bonded interfacial regions of immiscible polymer blends have lower activation energy for bubble nucleation.[26] This means that the interface in the immiscible blends could be favourable to the formation of nucleating sites for bubble growth. Thus the presence of a small amount of PS in LLDPE matrix (such as LLDPE/PS=90/10 or 80/20 blends) results in obviously increased cell density and expansion ratio compared to pristine LLDPE.

When the graft copolymer is added, the interfacial adhesion between two components will be strengthened. In the case of LLDPE/PS blends with co-continuous phase structure, the channel provided by interfacial region for the diffusion of dissolved CO_2 into the environment was blocked. Meanwhile, the enlarged surface areas and lower energy barrier were favourable for the bubble nucleation and growth of cell. Consequently, the introduction of 1.0 wt% PE-*g*-PS dramatically improved foaming behaviour of LLDPE/PS blends (such as LLDPE/PS=70/30 and 50/50 blends). In addition, as shown in Figure 1, the average size of the dispersed phase decreased with the content of PE-*g*-PS (also see Figure S3a). The increased interfacial areas promoted heterogeneous nucleation, resulting in the formation of more nuclei for foaming. Therefore, the cell density of foamed LLDPE/PS blends was dramatically increased with the content of PE-*g*-PS. Comparing the foam morphologies of LLDPE/PS/PE-*g*-PS blends (70/30/1.0–50/50/1.0) before with after etching by THF, it was found that a part of frame structure of the foams was uniformly etched by THF (Figure S11 in the supporting information). This indicated that the foam structure was composed of both LLDPE and PS, and it was difficult to distinguish the foam regions from LLDPE and PS. In contrast, the presence of PE-*g*-PS in LLDPE/PS blends with sea-island phase structure did not strongly change the foaming behaviour of LLDPE/PS blends, although the interfacial adhesion was improved. The phenomenon was ascribed to the interfacial region which was isolated in the blends with sea-island phase structure. In this case, whether adding compatibilizer or not will not influence the diffusion of CO_2 in the blend bulk.

Another interesting phenomenon observed in this work is that PS component formed foam structure in the binary LLDPE/PS=50/50 blend after foaming process. Poor interfacial adhesion between two components in LLDPE/PS=50/50 blend with co-continuous structure was very clear. Although a large amount of dissolved CO_2 escaped rapidly to the environment through the interface (large gap was also observed), the CO_2 dissolved in PS matrix could still nucleate and the cell grew. Very recently, the latest report has studied the unique microcellular skin-core structures embedded in PLA/PS foams.[43] It is thought that this interesting phenomenon of confined foaming behavior is involved in several factors, such as the weight ratio of components and phase structures (the shape and size of interface) of polymer blends, etc.

Conclusions

The foaming behaviour of LLDPE/PS blends with or without PE-*g*-PS as compatibilizer was studied by batch foaming. The compatibilization of PE-*g*-PS and the blend composition strongly affected the foaming behaviour of LLDPE/PS blends. When the content of one component (LLDPE or PS) was lower than 20 wt%, the morphology of LLDPE/PS blends presented sea-island structure. In this case, the blends showed improved foaming behaviours (i.e. decreased cell size and increased cell density) comparing with pure LLDPE and PS, but the addition of PE-*g*-PS did not further change the foam morphology of these blends. When the composition of LLDPE/PS blends was 70/30-30/70 by weight, the blends presented co-continuous phase structure. In this case, the binary blends showed very poor foaming ability. With the addition of PE-*g*-PS, the blends exhibited well foamed morphology, indicating dramatical improvement of foamability of these blends. This phenomenon did not show close relation with the change in melt viscosity of LLDPE/PS blends after adding the compatibilizer. The reasonable explanation was ascribed to consecutive state of interfacial region, resulting from different phase structure of the blends. The interfacial region is

isolated in the blends with sea-island phase structure (LLDPE/PS blends with the composition of 90/10, 80/20, 20/80 and 10/90). Otherwise, the interfacial region is consecutive in the blends with co-continuous phase structure (LLDPE/PS blends with the composition of 70/30–30/70). In the case of LLDPE/PS blends with co-continuous phase structure, as the consecutive interfacial region between two components (due to the poor interfacial adhesion) provided channels through which gas could rapidly diffuse from the blend bulk to the environment, the binary blends with co-continuous phase structure showed a poor foaming capability. The presence of PE-*g*-PS blocked the channel provided by interfacial region for the diffusion of dissolved CO_2 into the environment. However, the foam morphologies of the compatibilized blends by PE-*g*-PS with different PS length did not show obvious difference under the present foaming conditions. It is of interest that three kinds of foamed materials can be prepared from LLDPE/PS blends under the batching foaming process, depending on the blend composition and the compatibilization. Only the continouns component formed the foamed structure and the dispersed component acted as nucleating agent in the blends with sea-island phase structure. In contrast, both LLDPE and PS components in the blends with co-continuous phase structure were foamed in the comaptibilized blends, but only PS component was foamed in the binary blends (such as LLDPE/PS=50/50).

Acknowledgement

The financial supports from National Natural Science Foundation of China (51233005 and 21304089) and the Ministry of Science and Technology of China (SS2015AA031501) are greatly appreciated.

References

[a] *State Key Laboratory of Polymer Physics and Chemistry, Changchun Institute of Applied Chemistry, Chinese Academy of Sciences, Changchun 130022, China. Fax: +86(0)431 85262827; Tel: +86(0)431 85262004; E-mail: ttang@ciac.ac.cn*

[b] *Graduate School of the Chinese Academy of Sciences, Beijing 100039, China.*

† Electronic Supplementary Information (ESI) available: The details for the synthesis and characterization of PE-*g*-PS, the change trend of dispersed phase, morphologies of LLDPE/PS blends before and after foaming, and the plot of complex viscosity vs angular frequency. See DOI: 10.1039/b000000x/

1. D. Gersappe, D. Irvine, A. C. Balazs, Y. Liu, J. Sokolov, M. Rafailovich, S. Schwarz and D. G. Peiffer, *Science*, 1994, **265**, 1072.
2. G. Basseri, M. Mehrabi Mazidi, F. Hosseini and M. K. Razavi Aghjeh, *Polym. Bull.*, 2014, **71**, 465.
3. E. Van Hemelrijck, P. Van Puyvelde, C. W. Macosko and P. Moldenaers, *J. Rheol. (1978-present)*, 2005, **49**, 783.
4. S. Lyu, T. D. Jones, F. S. Bates and C. W. Macosko, *Macromolecules*, 2002, **35**, 7845.
5. P. Van Puyvelde, S. Velankar and P. Moldenaers, *Curr. Opin. Colloid In.*, 2001, **6**, 457.
6. M. Heino, J. Kirjava, P. Hietaoja and J. A seppälä, *J. Appl. Polym. Sci.*, 1997, **65**, 241.
7. C. W. Macosko, P. Guégan, A. K. Khandpur, A. Nakayama, P. Marechal and T. Inoue, *Macromolecules*, 1996, **29**, 5590.
8. U. Sundararaj and C. W. Macosko, *Macromolecules*, 1995, **28**, 2647.
9. A. Chirawithayaboon and S. Kiatkamjornwong, *J. Appl. Polym. Sci.*, 2004, **91**, 742.
10. I. Fortelný, J. Mikešová, J. Hromádková, V. Hašová and Z. Horák, *J. Appl. Polym. Sci.*, 2003, **90**, 2303.
11. P. Charoensirisomboon, T. Chiba, S. I. Solomko, T. Inoue and M. Weber, *Polymer*, 1999, **40**, 6803.
12. N. Kitayama, H. Keskkula and D. R. Paul, *Polymer*, 2000, **41**, 8041.
13. J. K. Kim and H. Lee, *Polymer*, 1996, **37**, 305.
14. T. Tang and B. Huang, *Polymer*, 1994, **35**, 281.
15. T. Tang, Z. Lei and B. Huang, *Polymer*, 1996, **37**, 3219.
16. L. Wang, H. Tan, J. Gong and T. Tang, *J. Appl. Polym. Sci.*, 2014, **131**, 40126.
17. T. Tang, Z. Lei, X. Zhang, H. Chen and B. Huang, *Polymer*, 1995, **36**, 5061.
18. S. Doroudiani, C. B. Park and M. T. Kortschot, *Polym. Eng. Sci.*, 1998, **38**, 1205.
19. H. Li, L. J. Lee and D. L. Tomasko, *Ind. Eng. Chem. Res.*, 2003, **43**, 509.
20. L. M. Matuana, C. B. Park and J. J. Balatinecz, *Polym. Eng. Sci.*, 1997, **37**, 1137.
21. T. Mizumoto, N. Sugimura, M. Moritani, Y. Sato and H. Masuoka, *Macromolecules*, 2000, **33**, 6757.
22. P. Zhang, N. Q. Zhou, Q. F. Wu, M. Y. Wang and X. F. Peng, *J. Appl. Polym. Sci.*, 2007, **104**, 4149.
23. K. Yao, H. Tan, Y. Lin, G. Zhang, J. Gong, J. Qiu, T. Tang, H. Na and Z. Jiang, *RSC Adv.*, 2014, **4**, 64053.
24. X. Han, J. Shen, H. Huang, D. L. Tomasko and L. J. Lee, *Polym. Eng. Sci.*, 2007, **47**, 103.
25. D. L. Tomasko, A. Burley, L. Feng, S.-K. Yeh, K. Miyazono, S. Nirmal-Kumar, I. Kusaka and K. Koelling, *J. Supercrit. Fluid.*, 2009, **47**, 493.
26. J. S. Colton and N. P. Suh, *Polym. Eng. Sci.*, 1987, **27**, 493.
27. P. Rachtanapun, S. E. M. Selke and L. M. Matuana, *J. Appl. Polym. Sci.*, 2003, **88**, 2842.
28. C. Zepeda Sahagún, R. González Núñez and D. Rodrigue, *J. Appl. Polym. Sci.*, 2007, **106**, 1215.
29. T. A. Walker, D. J. Frankowski and R. J. Spontak, *Adv. Mater.*, 2008, **20**, 879.
30. Q. Wu, C. B. Park, N. Zhou and W. Zhu, *J. Cell. Plast.*, 2009, **45**, 303.
31. H. Ruckdäschel, P. Gutmann, V. Altstädt, H. Schmalz and A. E. Müller, *Adv. Polym. Sci.*, 2010, **227**, 199.
32. P. Rachtanapun, S. E. M. Selke and L. M. Matuana, *Polym. Eng. Sci.*, 2004, **44**, 1551.
33. P. Rachtanapun, S. E. M. Selke and L. M. Matuana, *J. Appl. Polym. Sci.*, 2004, **93**, 364.
34. C. Z. Sahagún, R. González-Núñez and D. Rodrigue, *J. Cell. Plast.*, 2006, **42**, 469.
35. W. Zhai, H. Wang, J. Yu, J. Dong and J. He, *J. Polym. Sci. Part B: Polym. Phys.*, 2008, **46**, 1641.
36. *US Pat.*, 4 847 150, 1989.
37. Y. Xu, C. M. Thurber, T. P. Lodge and M. A. Hillmyer, *Macromolecules*, 2012, **45**, 9604.
38. M. A. Hillmyer, W. R. Laredo and R. H. Grubbs, *Macromolecules*, 1995, **28**, 6311.
39. K. A. Arora, A. J. Lesser and T. J. McCarthy, *Macromolecules*, 1998, **31**, 4614.
40. S. K. Goel and E. J. Beckman, *Polym. Eng. Sci.*, 1994, **34**, 1137.
41. G. Gedler, M. Antunes and J. I. Velasco, *J. Supercrit. Fluid.*, 2014, **88**, 66.
42. K. Goren, L. Chen, L. S. Schadler and R. Ozisik, *J. Supercrit. Fluid.*, 2010, **51**, 420.
43. X. Liao,. H. Zhang, Y. Wang, L. Wu and G. Li, *RSC Adv.*, 2014, **4**, 45109.

For Table of contents only

Interplay between the composition of LLDPE/PS blends and their compatibilization with polyethylene-*graft*-polystyrene in the foaming behaviour

Guangchun Zhang,[a,b] Yuanliang Wang,[a,b] haiping Xing,[a] Jian Qiu,*[a] Jiang Gong,[a,b] Kun Yao,[a,b] Haiying Tan,[a,b] Zhiwei Jiang,[a] Tao Tang*[a]

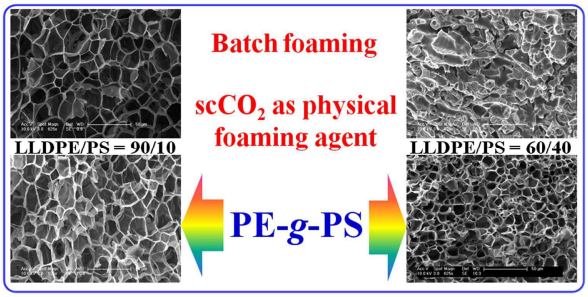

The influences of PE-*g*-PS compatibilization on the foaming behaviour of LLDPE/PS blends in batch foaming using $scCO_2$ as physical foaming agent depend strongly on the compostion of the blends.